Photoinduced Interactions in a Pyrene-Calix[4]arene-Perylene Bisimide Dye System: Probing Ground-State Conformations with Excited-State Dynamics of Charge Separation and Recombination

Nguyen Vân Anh,[†] Felix Schlosser,[‡] Michiel M. Groeneveld,[†] Ivo H. M. van Stokkum,*[,§] Frank Würthner,*[,‡] and René M. Williams*[,†]

Molecular Photonics Group, van't Hoff Institute for Molecular Sciences (HIMS), Universiteit van Amsterdam, Nieuwe Achtergracht 129, 1018 WV Amsterdam, The Netherlands, Institut für Organische Chemie and Röntgen Research Center for Complex Material Systems, Universität Würzburg, Am Hubland, D-97074 Würzburg, Germany, and Department of Physics and Astronomy, Vrije Universiteit, de Boelelaan 1081, 1081 HV Amsterdam, The Netherlands

Received: June 12, 2009; Revised Manuscript Received: August 25, 2009

A calix[4]arene scaffold has been functionalized with an electron-accepting perylene bisimide as well as an electron-donating pyrene unit. Steady-state and time-resolved spectroscopy indicate a strong charge-transfer (CT) interaction between these two units in all investigated solvents. The signatures of the radical anion of the perylene bisimide and the radical cation of the pyrene are observed with femtosecond transient absorption spectroscopy. A preferential π-stacked conformation is inferred. In tetrahydrofuran as a solvent ~25% of an extended form is invoked. The CT states of these two ground-state populations (π-stacked and extended) have different formation and decay kinetics and result in the spectral distinction of a compact and an extended charge-transfer state upon visible excitation. In the extended conformation, upon UV excitation, pyrene acts as an electron acceptor that is reduced through a photoinduced electron-transfer process by the calix[4]arene. In this conformation the calixarene scaffold is accordingly not an uninvolved linker unit but participates effectively in the electron-transfer processes.

Introduction

The development of photoactive organized dye systems for directional excitonic and electronic transport is important for generating new organic photonic applications and electro-optical devices.[1] An important step in this direction was taken by Tang et al.,[2] who reported the first two-layer organic solar cell containing 3,4:9,10-perylene tetracarboxylic bis(benzimidazole) as the n-type material and copper phthalocyanines as the p-type counterpart. Recent work on polymer-C_{60} solar cells has shown that generating a nanoscopic interpenetrating network is essential for good device operation (for, e.g., PCBM-PPV).[3] Next to controlling the physics of phase separation, self-organization of electron donor−acceptor systems with supramolecular functionality is a means toward creating nanoscopic networks.[4] Examples of supramolecular recognition and organization applied in materials science are represented by hydrogen-bonded polymer systems[5] as well as cyclodextrin-functionalized fabrics[6] and dyes.[7] The self-organization can, in principle, be attained by introduction of a supramolecular unit that can be used to induce a secondary structure.

Toward this direction, we recently reported[8] on energy-transfer cascades in calixarene-linked dye systems containing orange-, red-, and green-colored perylene bisimide chromophores. The 3,4:9,10-perylene tetracarboxylic bis(dicarboximides) dyes (PBI) are excellent highly absorbing and photostable organic dyes for such purposes for which the absorption spans a large part of the solar spectrum.[9] This class of compounds is also applied as laser dyes[10] in xerography and in car paints.[11] The simplest supramolecular building block of our calixarene−PBI series[12] (the orange-colored PBI "perylene orange" linked to a calix[4]arene) as well as calixarenes bearing two identical PBIs[13] have been studied. Here we report on progress toward charge separation in such cascade systems by introducing an electron-donating pyrene chromophore into the calixarene-linked system (see Figure 1).

The combination of the textbook-chromophore pyrene[14] with the third generation of supramolecular hosts[15] has been applied before. The excimer emission of calixarenes functionalized with two pyrene units[16] has been used in various ion-sensing modalities. Whereas "bare" perylene and pyrene have been grafted together onto one calix[17] previously, the combination of PBI dyes and pyrene onto this scaffold is unprecedented.

We show that the excited-state dynamics of **Py-c-PBI** is characterized by charge-transfer interactions in all solvents (with polarities ranging from cyclohexane to acetonitrile). Charge-transfer absorption bands and optical electron transfer are observed. In tetrahydrofuran (and to a minor extent in benzonitrile) two ground-state populations are discovered that arise from specific solute−solvent interactions. These two ground-state populations exhibit different formation and decay kinetics and result in the spectral distinction of a compact and an extended charge-transfer state.

* To whom correspondence should be addressed. E-mail: R.M.Williams@uva.nl (R.M.W.); wuerthner@chemie.uni-wuerzburg.de, (F.W.); ivo@few.vu.nl, (I.H.M.v.S.).
[†] Universiteit van Amsterdam.
[‡] Universität Würzburg.
[§] Vrije Universiteit.

10.1021/jp9055279 CCC: $40.75
Published on Web 09/25/2009

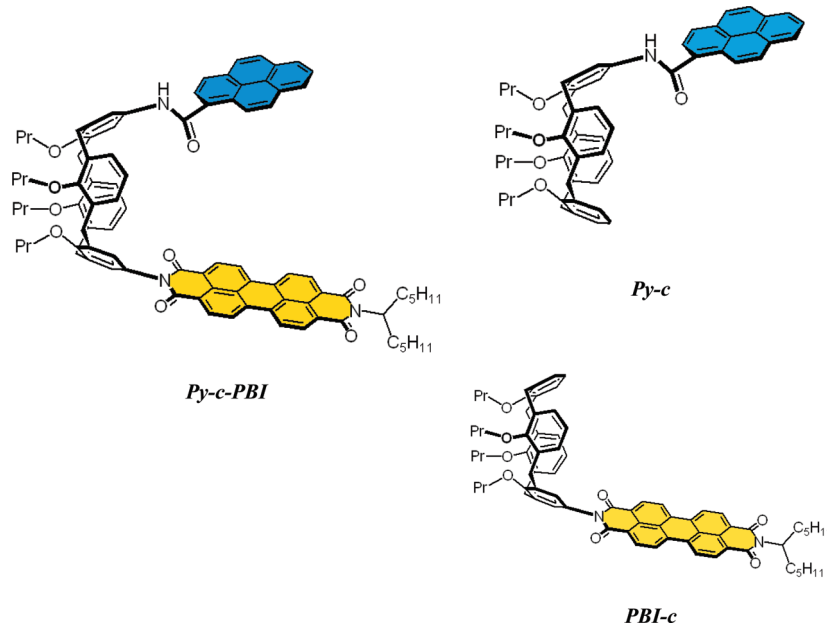

Figure 1. Molecular structure of the **Py-c-PBI** system containing a carboxamido-pyrene unit (**Py**) linked to a calix[4]arene (**c**) functionalized with **PBI** ("perylene orange"). Also shown are the reference compounds **Py-c** and **PBI-c**.

Experimental Section

Sample Preparation. The molar absorption coefficient (ε) of **Py-c-PBI** in dichloromethane was determined gravimetrically to be 62 900 M^{-1} cm^{-1} at 533 nm. The values of ε in other solvents were determined by preparing solutions of known concentration from a stock solution of millimolar concentrations of **Py-c-PBI** in dichloromethane of which the concentration was determined spectrophotometrically based on the above value of ε. The ratio of the stock solution is not more than 0.5% in volume. All solvents were purchased from Aldrich, Acros, or Merck with spectrophotometric or HPLC grade and used as received. For the absorption and fluorescence measurements, the spectra of solvents were recorded before the samples were prepared to ensure the absence of interference. For femtosecond transient measurements, the samples were filtered (0.4 μm PVDF filters) to remove particles and had an absorbance of ca. 0.15−0.2 at the excitation wavelength using 2 mm cells. The UV−vis absorption spectra of the samples were measured before and after the laser experiments and found to be virtually identical, thus ruling out a possible degradation or chemical change of the samples.

Steady-State Absorption and Fluorescence Measurements. Electronic absorption spectra were measured in a quartz cuvette (1 cm, Hellma) on a Cary 300 spectrophotometer for determining molar absorption coefficients and absorbance of samples for quantum yield measurements. Steady-state fluorescence spectra were recorded on a SPEX Fluorolog 3-22 fluorimeter, equipped with a Xe arc light source, a Hamamatsu R636-10 photomultiplier tube detector, and double excitation and emission monochromators using a 475 nm cutoff filter (emission) for perylene emission and a 345 nm cutoff filter (emission) for pyrene emission.

Fluorescence quantum yields[18] were measured in optically dilute solutions (<10^{-6} M) using the indicated reference solutions according to the following equation

$$\Phi_u = [(A_r I_u n_u^2)/(A_u I_r n_r^2)]\Phi_r$$

where u and r denote the unknown and reference, Φ is the quantum yield, A is the absorbance (0.07−0.1 using 10 mm cuvette) at the excitation wavelength, I is the integrated emission intensity, and n is the refractive index of the solvent(s). *N*,*N*′-Bis(2,5-di-*tert*-butylphenyl)-3,4:9,10-perylenedicarboximide (DBPI; fluorescence quantum yield is 0.99 in chloroform)[19] and anthracene (0.27 in ethanol)[20] were used as the standard for perylene emission and pyrene, respectively.

In order to determine the very small quantum yield of the perylene emission of **Py-c-PBI** with higher accuracy a neutral density filter (ND 1.0, Schott) was used in the excitation pathway for measurement of the reference (but was taken out for the sample measurement while using the same system configuration). Using the absorption of the ND filter at the excitation wavelength ($A_{470\ nm} = 0.96$) the quantum yield of **Py-c-PBI** was determined. The effect of the ND filter on the emission intensity of the reference was verified first and in good accordance with the ND filter effect (reducing its emission intensity with a factor 10^{-A}). The estimated error of applying this method for determination of very low quantum yields is less than 5% (by using this comparison). This method allowed measurements with excitation and emission slits of 12 and 2 nm, respectively (these setting would normally overload our detector for this reference compound). Integration times of 1 s and increments of 1 nm were used. No correction was applied to the fluorescence spectra.

Femtosecond Transient Absorption (FTA). FTA experiments were performed with a Spectra-Physics Hurricane Titanium:Sapphire regenerative amplifier system. The full spectrum setup was based on an optical parametric amplifier (Spectra-Physics OPA 800C) as the pump. The residual fundamental light, from the pump OPA, was used for white light generation, which was detected with a CCD spectrograph (Ocean Optics PC2000 + slave) for visible detection. The polarization of the pump light was controlled by a Berek Polarization Compensator (New Focus). The Berek Polarizer was always included in the setup to provide the magic-angle conditions. The probe light was double passed over a delay

SCHEME 1: Synthesis of the Py-c-PBI System 5[a]

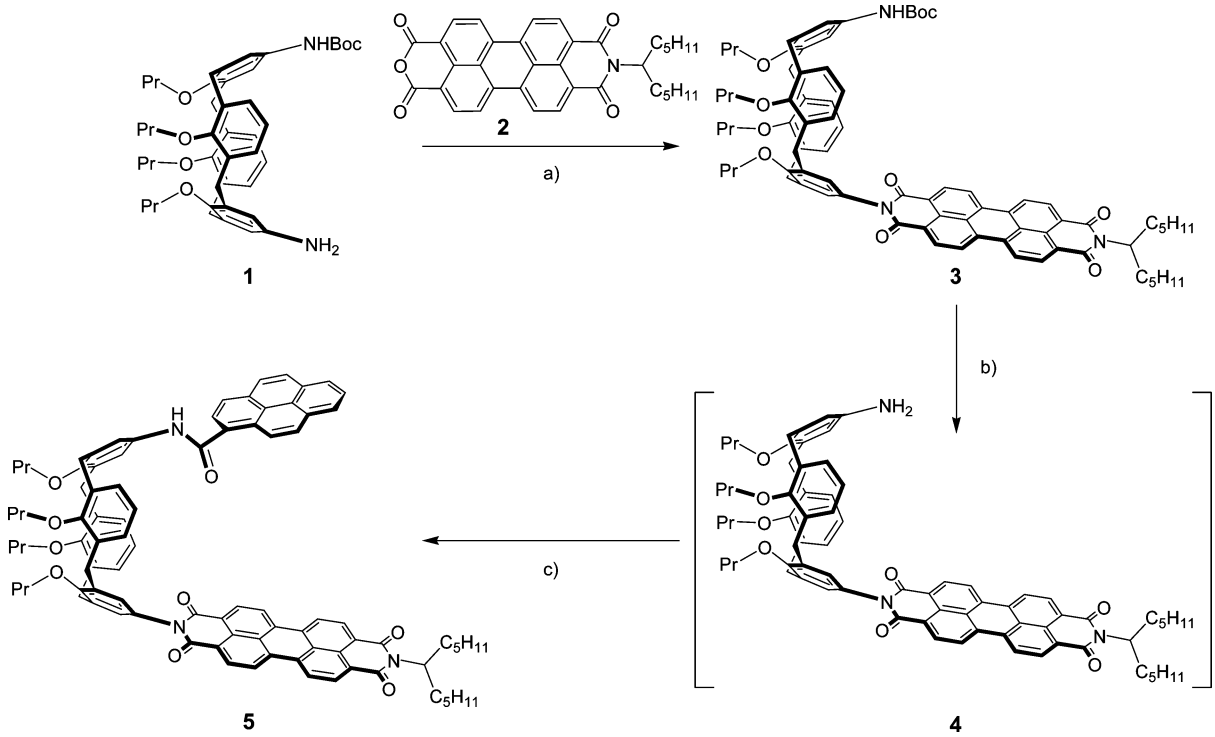

[a] Reagents and conditions: (a) Et_3N, toluene, reflux, yield 58%; (b) CF_3COOH, CH_2Cl_2, rt; (c) 1-pyrenecarboxylic acid, *N*-methylmorpholine (NMM), *N*,*N*′-dicyclohexylcarbodiimide (DCC), 1-hydroxybenzotriazole (HOBt), DMF, CH_3CN, rt, yield 33% over two steps.

line (Physik Instrumente, M-531DD) that provides an experimental time window of 3.6 ns with a maximal resolution of 0.6 fs/step. The OPA was used to generate excitation pulses at 350 or 530 nm. The laser output was typically 3.5−5 μJ pulse^{-1} (130 fs fwhm) with a repetition rate of 1 kHz. The samples were placed into cells of 2 mm path length (Hellma) and stirred with a downward projected PTFE shaft using a direct drive spectro-stir (SPECTRO-CELL). This stir system was also used for the white light generation in a 2 mm water cell. For femtosecond transient absorption in the NIR region a Control Development NIR-256 L-1.7T1-USB, optical spectrometer system, InGaAs detector with 512 element arrays responding to wavelengths in the range from 900−1700 nm, was used. Detection light was generated with a sapphire plate.

All photophysical data reported here have a 5−10% error limit. All experiments were performed at room temperature.

Molecular Modeling. Molecular modeling was performed with the Spartan′04 V1.03 package (Wave function Inc.). The molecule was first built in two forms, extended and π-stacked; then equilibrium conformers were calculated using the molecular mechanics method on the MMFF level to get the initial structures. Next, geometry optimization was performed using the semiempirical AM1 method.

For the global and target analysis[21] all time-gated spectra were collated in a matrix, which was globally fitted using a sequential kinetic scheme with increasing lifetimes. From this the lifetimes and evolution-associated difference spectra (EADS) were estimated. The instrument response function (IRF) is described by a Gaussian shape, and the white light dispersion over the spectral range is modeled by a third-order polynomial. With increasing lifetimes and thus decreasing rates, the first EADS decays with the first lifetime and corresponds to the difference spectrum at time zero with an ideal infinitely small IRF. The second EADS is formed with the first lifetime and decays with the second lifetime, etc. The final EADS represents the difference spectrum of the longest living species. The error in the lifetimes obtained from the fitting procedure does not exceed 10%. EADS may not represent pure species except for the final EADS, and they are interpreted as a weighted sum (with only positive contributions) of species-associated difference spectra (SADS). The quality of the fit was judged by inspection of the singular vectors of the matrix of residuals, which had to be structureless. Next, in target analysis a kinetic scheme was used in combination with spectral assumptions to estimate microscopic rate constants and SADS.

Results and Discussion

Synthesis. The **Py-c-PBI** system **5** was synthesized in three steps according to Scheme 1. For this purpose, the mono-Boc-protected calix[4]arene **1**[22] was reacted with the perylene monoimide (PMI) **2** in refluxing toluene/Et_3N to yield compound **3** in 58%. Deprotection of the amino group in **3** with trifluoroacetic acid was followed by an amide coupling with 1-pyrenecarboxylic acid in DMF/acetonitrile using *N*-methylmorpholine (NMM), *N*,*N*′-dicyclohexylcarbodiimide (DCC), and 1-hydroxybenzotriazole (HOBt) to afford the desired conjugate **5** in 33% yield over two steps. Compound **5** was properly characterized by ^{1}H NMR, ^{13}C NMR, and high-resolution mass spectrometry (HR-MS). The details are given in the Supporting Information, where also the **Py-c** reference system is described. It can be noted that the NMR signals of the pyrene signals of **Py-c-PBI** range from 6.98 to 8.02 ppm, whereas the data of **Py-c** range from 8.16 to 8.55 ppm (see the Supporting Information).

Molecular Modeling. From the Lewis structure of **Py-c-PBI** (Figure 1) it can be envisaged that this three-component system can adopt two conformations attributed to the two possible pinched-cone conformations of the calix[4]arene: the system can adopt a π-stacked form and an extended form.

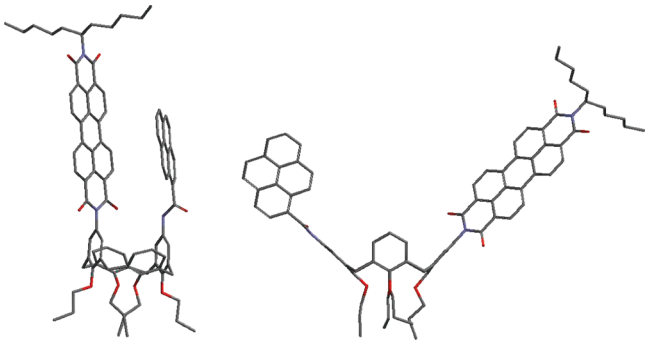

Figure 2. Two possible conformers of **Py-c-PBI** (π-stacked and extended). Hydrogens are omitted.

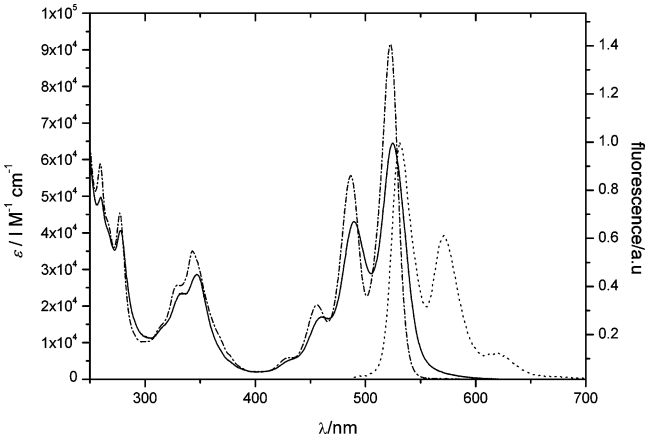

Figure 3. Absorption (solid line) and fluorescence spectra (dotted line) of **Py-c-PBI** in THF together with the sum spectrum (dash−dot line) of the two separate reference chromophores DBPI and **Py-c**. For a comparison of **Py-c**, **PBI-c**, and **Py-c-PBI** in dichloromethane, see Figure S2.13 (Supporting Information).

Figure 2 shows calculated equilibrium geometries of the π-stacked conformation in which two aromatic chromophores are in face-to-face position and the extended conformer of **Py-c-PBI** in which the two substituents are farther away from each other.

Electronic Properties. The absorption and emission spectra of **Py-c-PBI** in tetrahydrofuran (THF), as shown in Figure 3, are characterized by the typical PBI absorption (525, 490, and 461 nm) and emission (530, 580, and 640 nm) peaks of the PBI chromophore in the visible region. A good mirror image can be observed with a very small Stokes shift, indicating only a small geometrical reorganization of the chromophore in the excited state.

In the UV region the peaks of the pyrene at ca. 347 and 333 nm can be clearly discerned.[23] It can be noted that the amide functionality modulates the fine structure and intensity of the absorption to the pyrene singlet states. Similar effects have been described before.[24]

Comparison with the sum spectrum of the two separate chromophores shows a strong perturbation due to interaction between the pyrene and PBI units in the ground state (see also the Supporting Information for comparison of **Py-c**, **PBI-c**, and **Py-c-PBI** in dichloromethane).

A clear broadening of the PBI absorption peaks is accompanied by a reduction in the molar absorption coefficients for the peak maxima, as compared to reference systems,[12,19] indicating ground-state interaction. A charge-transfer absorption band is present in the visible range (between 500−600 nm); however, it strongly overlaps with the PBI absorption bands, preventing deduction of (the maximum of) a structureless charge-transfer absorption band. Absorption and emission data of **Py-c-PBI** in other solvents are presented in Table 1.

Strong indications for excited-state interactions are provided by the fluorescence quantum yields (Φ_F) for **Py-c-PBI** (Figure 4, Table 1). The Φ_F values indicate a very strong quenching of the perylene unit in **Py-c-PBI** (Φ_F ranges from 4×10^{-4} to 2.6×10^{-3}) in comparison with the perylene bisimide chromophore itself (Φ_F is near unity). These quantum yields are also substantially smaller than those of the calix[4]arene-functionalized PBI[12] (quantum yields of ~0.02−0.03 for **PBI-c**). By taking **Py-c-PBI** in $CHCl_3$ as a reference point, it can be seen that the fluorescence quantum yields of **Py-c-PBI** in phCN, THF, and TOL are up to six times higher than in the other solvents.

In all seven solvents the fluorescence quantum yields of the pyrene moiety of **Py-c-PBI** are less than 10^{-4} and, thus, at the detection limit. By contrast, the quantum yield of pyrene in cyclohexane[23] is 0.65; that of amide-functionalized pyrene[24] is 0.64. For calix[4]arene-pyrene (**Py-c**) Φ_F is ca. 1×10^{-3} (see the Supporting Information).

The steady-state spectroscopy of **Py-c-PBI** shows that the molar absorption coefficients and luminescence quantum yields are strongly affected by the interaction of the pyrene with the PBI unit in low- and high-polarity solvents. It appears that both in the ground state and in the excited state interaction occurs, the former being indicated by the changed absorption properties. As charge separation is envisaged to occur in these molecules, with pyrene as the donor and PBI as the acceptor, time-resolved spectroscopy was applied to provide more information on this process.

Femtosecond Transient Absorption. The transient absorption spectra of **Py-c-PBI** in THF probed in the visible region and excited at 350 (pyrene excitation) or 530 nm (PBI excitation) (see Figure 5a and 5b) are rather similar. The spectra show the characteristic features of the PBI unit with strong ground-state bleaching at ca. 492 and 527 nm, the absorption of PBI anion at the band centered at 710 nm,[12,25] which overlaps with the PBI singlet excited state.[12,26] Also, the pyrene radical cation absorption band at around 400−450 nm can be identified.[27] Spectra with these two characteristic features were observed in five other solvents of different polarity (see Figures S2.5−S2.9, Supporting Information).

When we compare transient absorption spectra upon visible excitation with those of **PBI-c**,[12] it is noticed that the emission of the PBI is much less pronounced in **Py-c-PBI**. This illustrates the ultrafast charge separation that occurs upon visible excitation. As discussed before, the emission quantum yields show that very strong quenching of the PBI unit of **Py-c-PBI** is prominent in all solvents (Table 1) but relatively weaker in THF, benzonitrile, and toluene.

The transient absorption spectra (Figure 5b) observed in THF (the solvent with the highest emission quantum yield, Φ_{PBI}) indicate the existence of an extended conformation of **Py-c-PBI** that shows a slightly slower charge separation process (see later). The spectra observed in all other solvents show even less emission (as a negative feature around 580 nm, see Figures S2.5−S2.9, Supporting Information) irrespective of solvent polarity and are all characteristic for charge separation.

Closer inspection of the data obtained with 350 nm excitation (as compared to 530 nm) in THF (Figure 5a) indicates some remarkable distinctions that are in agreement with pyrene excitation as well as a small amount of energy

TABLE 1: Absorption and Fluorescence Properties of Py-c-PBI in Seven Solvents

	absorption	fluorescence			
solvent	λ (nm); (ε, $M^{-1}cm^{-1}$)	λ_{PBI} [a](nm)	Stokes shift (cm^{-1})	Φ_{PBI}[a] (relative)	Φ_{py}[b]
CHX	278, 333, 347 (25 200)			5×10^{-4} (120)	$\leq 10^{-4}$
	459, 489, 525 (64 700)	525	0		
TOL	334, 350 (27 500)			1.2×10^{-3} (275)	$\leq 10^{-4}$
	466, 496, 533 (63 900)	538	174		
$CHCl_3$	279, 335, 350 (23 600)			4×10^{-4} (100)	$\leq 10^{-4}$
	466, 497, 534 (64 600)	538	139		
THF	278, 333, 347 (28 600)			2.6×10^{-3} (590)	$\leq 10^{-4}$
	460, 490, 525 (64 500)	531	215		
DCM	279, 334, 349 (23 300)			4×10^{-4} (85)	$\leq 10^{-4}$
	466, 496, 533 (62 900)	536	105		
phCN	336, 351 (26 100)			2.5×10^{-3} (550)	
	468, 499, 536 (62 400)	539	104		
ACN	278, 333, 348 (21 700)			5×10^{-4} (110)	$\leq 10^{-4}$
	465, 494, 531 (60 650)	531	0		

[a] $\lambda_{exc} = 470$ nm, excitation and emission slits of 12 and 2 nm, respectively; integration time of 1 s. [b] $\lambda_{exc} = 320$ nm, excitation and emission slits of 12 and 2 nm, respectively; integration time of 1 s. CHX: cyclohexane. TOL: toluene. $CHCl_3$: chloroform. THF: tetrahydrofuran. DCM: dichloromethane. phCN: benzonitrile. ACN: acetonitrile.

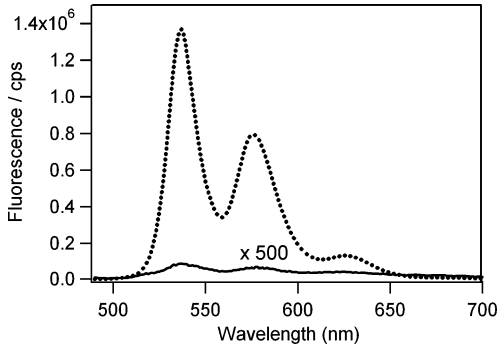

Figure 4. Fluorescence spectra of **Py-c-PBI** (solid line, multiplied by 500) together with the reference (DBPI) compound (dotted line) in $CHCl_3$. In the determination of the emission ratios of DBPI and **Py-c-PBI**, a neutral density filter was employed (see Experimental Section).

transfer from the pyrene unit to the PBI unit. At 2 ps it is clear that the negative PBI bleach is superimposed onto a broader positive absorption centered around at ~500 nm. The ~500 nm band is assigned to excited-state absorption of pyrene[27,28] as well as the pyrene radial anion (490−520 nm).[29] Also, features of the S_2-S_n pyrene absorption (500−580 nm)[27,30,31] can be extracted from the data (see next section). The observation of some PBI emission (around 580 nm) upon pyrene excitation provides evidence for some energy transfer from the pyrene singlet excited state to the PBI chromophore on a (sub)picosecond time scale in the extended conformer.

The transient absorption spectra of **Py-c-PBI** in THF with NIR detection (Figure 5c and 5d) are characterized by the second PBI radical anion band[12,25] that is centered at 958 nm. This is in agreement with formation of a charge-separated state. Upon 530 nm excitation the singlet PBI absorption with the broad band at 900−1000 nm[32] is also present at very early times (see also global analysis section). The spectra of **Py-c-PBI** in THF with NIR detection confirm that ultrafast electron transfer takes place at both 350 and 530 nm excitation. For **Py-c-PBI** in the other solvents similar events can be observed (see Figures S2.5−S2.9, Supporting Information).

Global and Target Analysis of Visible Excitation. The combined femtosecond transient absorption data matrices of **Py-c-PBI** obtained with visible or NIR detection (530 nm excitation) were analyzed with spectrotemporal parametrization[21] in five solvents. A target model that implies ultrafast charge separation followed by fast solvation (with some minor competing charge recombination) and subsequent charge recombination appropriately describes the data in all solvents except in THF. In the latter solvent, in which the highest steady-state luminescence intensity was observed also, a more elaborate model was applied. In THF the presence of two coexisting conformations was invoked, an extended (25%) and a π-stacked (75%) conformation. In the extended conformation charge separation and charge recombination are slower. The applied models are represented in Figure 6.

Figure 7 exemplifies the species-associated difference spectra that are attributed to the first excited singlet state of the PBI and the different charge-transfer states (e.g., CT_1 and CT_2). The first excited singlet state of the PBI is characterized by ground-state bleaching and emission (with a typical negative pattern with peaks at 490, 527, and 574 nm), an absorption band at around 700 nm, and a broad absorption band in the NIR region at ~910 nm, both attributed to the $S_1 \rightarrow S_n$ absorption.[12,32] The charge-transfer state described by the reduced PBI and the oxidized pyrene unit is characterized by a strong ground-state bleaching (490 and 527 nm), the total absence of PBI-based emission, the radical anion absorption features at 720 nm (broad) and 955 nm (sharp), as well as weak radical cation features of the pyrene at ~400−450 nm.

Interestingly, the radical anion features of the extended form are sharper than the π-stacked form. This implies spectral differentiation between an extended charge-transfer state and a compact charge-transfer[33] state by transient absorption spectroscopy. Table 2 summarizes the outcome of the target analysis in the five solvents. The SADS are reported in the Supporting Information. Only for DCM as a solvent is a structural reorganization of the CT_2 state, leading to the CT_3 state, invoked.

It is important to notice that a photoinduced charge separation has also been observed in the model system **PBI-c**.[12] Compared to **Py-c-PBI**, charge separation in **PBI-c** occurs much slower (τ_{cs} ranges from 25 to 64 ps for **PBI-c**). In another study on calix[4]arenes bearing two identical PBI chromophores the coexistence of two conformations in nonpolar solvents could be proven by fast spectroscopy and confirmed by force field calculations.[13]

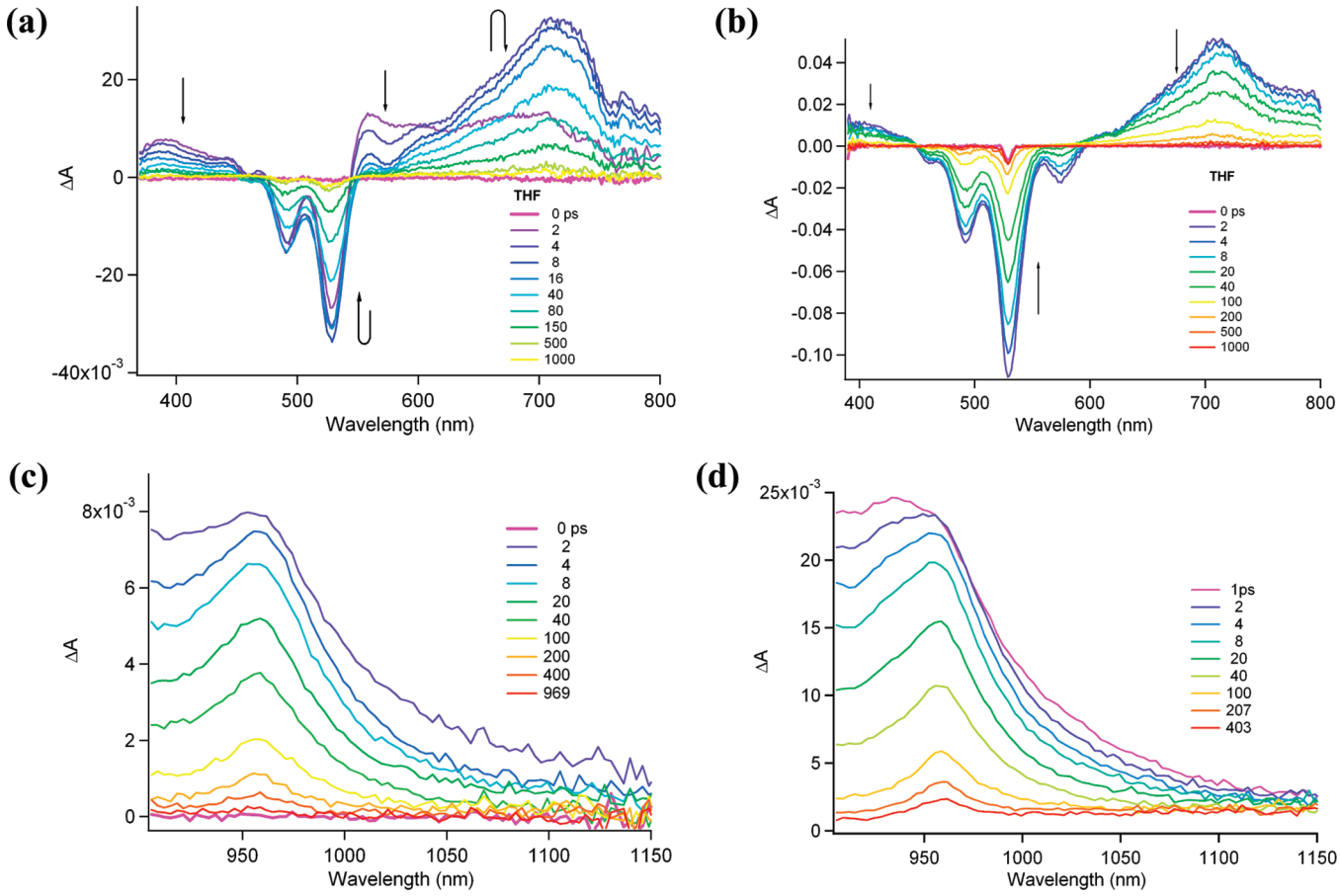

Figure 5. Femtosecond transient absorption spectroscopy of **Py-c-PBI** in THF: (a) $\lambda_{exc} = 350$ nm, (b) $\lambda_{exc} = 530$ nm, visible detection (c) $\lambda_{exc} = 350$ nm, NIR detection, and (d) $\lambda_{exc} = 530$ nm, NIR detection.

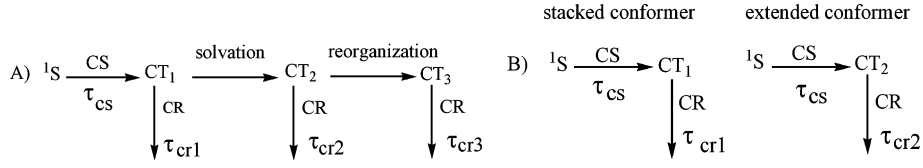

Figure 6. Two models, sequential (A) and parallel (B), used in target analysis upon 530 nm excitation.

Excited-State Properties of Pyrene-calix, Py-c. In order to clarify the excited-state properties of **Py-c-PBI** that play a role upon UV excitation it is needed to expand on the properties of **Py-c**. As stated before, the emission of **Py-c** is strongly quenched (relative to, e.g., amide-functionalized pyrene), and this must be due to the presence of the electron-donating calix[4]arene.

The femtosecond transient absorption spectra (Figure 8) of **Py-c** excited at the $S_0 \rightarrow S_2$ transition of the pyrene moiety (350 nm) display evidence of the electron-transfer process in which the calixarene acts as the electron donor. The absorption band at a delay time of 2 ps with a maximum at 550 nm is known as the $S_1 \rightarrow S_n$ absorption of the pyrene unit. The band peaking in the region 490−520 nm after 4 ps can be assigned to the pyrene radical anion.[29]

The global and target analysis (Figure 9) of the whole data matrix associated with Figure 8 indicates the presence of four species: the second and first excited singlet states of pyrene (S_2 and S_1) and the two charge-transfer states (CT_1 and CT_2). The S_2 state is created within the laser pulse and then decays via two possible channels. One is ultrafast internal conversion from S_2 into S_1 of pyrene;[28,30] the other is electron transfer from calixarene to pyrene. Part of the newly formed charge-transfer state (CT_1) undergoes a solvation process to the CT_2 state. These two charge-transfer states then decay to the ground state via a fast charge recombination process.

In summary, the excited-state behavior of **Py-c** is characterized by very fast charge separation from the calixarene to the pyrene followed by fast charge recombination.

Energetic Considerations. The Gibbs energy of photoinduced electron transfer ($\Delta_{ET}G°$) in a solvent with relative permittivity ε_s can be estimated by the equation (written here for neutral starting species)[34]

$$\Delta_{ET}G° = e[E°(D^{+\cdot}/D) - E°(A/A^{-\cdot})] - \Delta E_{0,0} - e^2/4\pi\varepsilon_o\varepsilon_s R_c - e^2/8\pi\varepsilon_o(1/r^+ + 1/r^-)(1/\varepsilon_{EC} - 1/\varepsilon_s) \quad (1)$$

For the **Py-c-PBI** system, the standard electrode potentials ($E°(D^{+\cdot}/D)$ and $E°(A/A^{-\cdot})$ of the donor (D) and acceptor (A) are +0.90 (Py/Py^+) and −1.09 V vs Fc/Fc^+ (PBI/PBI^-), respectively, in the reference solvent dichloromethane with a relative permittivity ε_{EC} of 8.93 (for cyclic voltammetry, see Supporting Information). The zero−zero transition energy $E_{0,0}$ of the chromophore slightly varies with solvent. The center-to-center distance R_{cc} between the donor and the acceptor was determined from geometries of **Py-c-PBI**

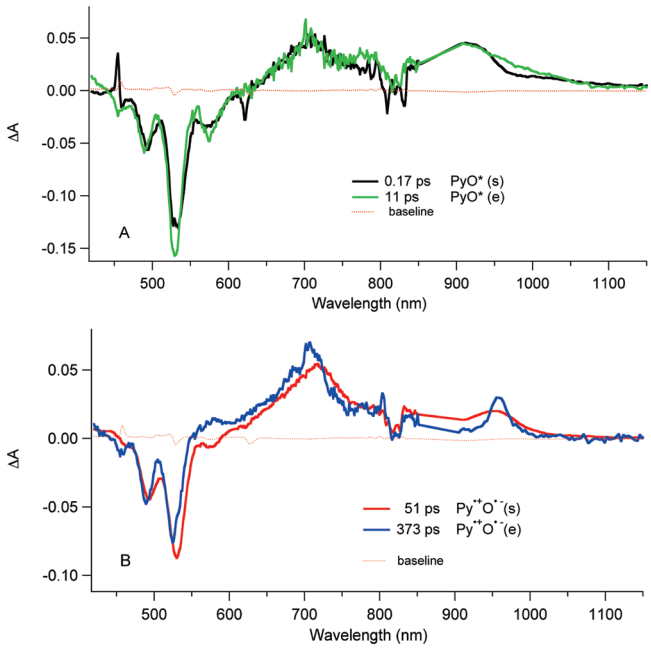

Figure 7. SADS (species-associated difference spectra) of the (A) first excited singlet state of **PBI** and (B) charge-transfer state of the stacked (s) and extended (e) conformations of **Py-c-PBI** in THF upon 530 nm excitation (visible and NIR detection) obtained with target analysis.

TABLE 2: Lifetimes of the Processes Occurring in Py-c-PBI Extracted from Global and Target Analysis (excitation at 530 nm)[a]

solvent	τ_{cs} (ps)	τ_{cr1} (ps)	τ_{cr2} (ps)	τ_{cr3} (ps)
CHX	0.10	4	19	
TOL	0.2	10	12	
THF (s)	0.17	51		
THF(e)	11	373		
DCM	0.10	1.6	16	50
ACN	0.10	1.4	88	

[a] In THF data is given for the stacked (s) and extended (e) conformation. In all other solvents only the stacked conformation is present. CHX: cyclohexane. TOL: toluene. THF: tetrahydrofuran. DCM: dichloromethane. ACN: acetonitrile.

optimized using a semiempirical AM1 method giving a value of 5.6 Å for the stacked conformer and 17.7 Å for the extended conformer. The effective radii of the donor (r^+) and acceptor (r^-) are estimated using a spherical approach.[35] These values are 3.98 Å for pyrene[36] (density 1.271 g/cm^3) and 4.78 Å for PBI[37] (density 1.407 g/cm^3). The results are shown in Table 3. The rates of the charge separation (CS) of **Py-c-PBI** in different solvents were determined theoretically by applying the Arrhenius equation

$$k_{et} = A \exp(-\Delta G^{\ddagger}/k_B T) \qquad (2)$$

in which k_B is the Boltzmann constant, T is the temperature, and $\Delta G^{\ddagger}$ is the Gibbs activation energy of the charge separation process. The pre-exponential factor A in eq 2 depends on the nature of the process (e.g., intermolecular or intramolecular electron transfer). We assume that for the system **Py-c-PBI**, A is constant with a value of 10^{13} s^{-1} in all solvents.[38] The Gibbs energy of activation ($\Delta G^{\ddagger}$) and the driving force ($\Delta G_{cs} = \Delta_{ET}G^{\circ}$) of the charge separation process are correlated using the eq 3[39]

$$\Delta G^{\ddagger} = (\Delta G_{cs} + \lambda)^2/4\lambda \qquad (3)$$

where λ is the reorganization energy consisting of solvent reorganization (λ_s) and internal reorganization (λ_i) energies, $\lambda = \lambda_i + \lambda_s$. The internal reorganization energy was assumed to be $\lambda_i = 0.2$ eV.[40] Using the Born−Hush approach,[35] the solvent reorganization energy (λ_s) is expressed as

$$\lambda_s = e^2/(4\pi\varepsilon_o)(1/r - 1/R_{cc})(1/\varepsilon_{op} - 1/\varepsilon_s) \qquad (4)$$

In this equation, ε_{op} ($= n^2$) and ε_s are the optical and static dielectric constants of the medium, $r = (r^+ + r^-)/2$. With these parameters, the barrier as well as the rate constants of the charge separation process taking place in the **Py-c-PBI** system in several solvents were estimated and are shown in the Tables 3 and 4. An estimate of the energetics of **Py-c** is given in the Supporting Information.

The charge separation (CS) rate constant also can be evaluated from the fluorescence quantum yield Φ_f as follows. The processes occurring in the parent chromophore (i.e., pyrene itself or DBPI in the case of the **Py-c-PBI** system) after excitation are fluorescence, relaxation to the ground state (internal conversion), and intersystem crossing to the triplet state with rate constants k_f, k_{ic}, and k_{isc}, respectively. Then, the fluorescence quantum yield and fluorescence lifetime (τ_f) are determined by the following expressions

$$\Phi_f^{ref} = \frac{k_f}{k_f + k_{ic} + k_{isc}}$$

$$\tau_f^{ref} = \frac{1}{k_f + k_{ic} + k_{isc}}$$

If the electron transfer (k_{cs}) in an electron donor-acceptor system is energetically allowed, the fluorescence quantum yield is lowered to Φ_f and the lifetime is decreased to τ_f

$$\Phi_f = \frac{k_f}{k_f + k_{ic} + k_{isc} + k_{cs}}$$

$$\tau_f = \frac{1}{k_f + k_{ic} + k_{isc} + k_{cs}}$$

Thus, we can determine the charge separation rates (k_{cs}) using the equations

$$k_{cs} = \frac{1}{\tau_f} - \frac{1}{\tau_f^{ref}} \quad k_{cs} = (\Phi_f^{ref}/\Phi_f - 1)/\tau_f^{ref}$$

For the PBI chromophore, the fluorescence quantum yields in various solvents are almost unity, $\Phi_f \approx 1$, and the fluorescence lifetime is also unchanged, $\tau_f \approx 4$ ns.[19] The charge-transfer rates estimated via the fluorescence quantum yield of PBI in several solvents are collected in Table 4. These rates are slower than those obtained from the global analysis results because the "real" emission quantum yields are most likely smaller (they are at the edge of the detection limit in the fluorescence measurements and less accurate than the global analysis results). By combining the outcome of the spectroscopy upon visible excitation with the driving force calculations in Table 3 we can create a coherent representation of the excited-state processes occurring in **Py-c-PBI**.

TABLE 3: Driving Force for Charge Separation (ΔG_{cs}) and Gibbs Energy of Activation ($\Delta G^{\ddagger}$) of the Py-c-PBI System upon PBI (A) Excitation in Different Solvents

				π-stacked conformer			extended conformer		
solvent	ε^a	n^b	$E_{0,0}{}^c$ [Per] (eV)	ΔG_{cs} (eV)	λ (eV)	$\Delta G^{\ddagger}$ (eV)	ΔG_{cs} (eV)	λ (eV)	$\Delta G^{\ddagger}$ (eV)
CHX	2.02	1.43	2.36	−0.39	0.20	0.040	0.49	0.19	0.61
TOL	2.38	1.49	2.31	−0.38	0.22	0.029	0.36	0.26	0.37
$CHCl_3$	4.86	1.44	2.31	−0.54	0.39	0.014	−0.17	0.87	0.14
THF	7.58	1.41	2.35	−0.63	0.47	0.014	−0.40	1.12	0.12
DCM	8.93	1.42	2.32	−0.61	0.47	0.011	−0.42	1.14	0.11
phCN	25.20	1.53	2.30	−0.66	0.48	0.017	−0.59	1.16	0.07
ACN	35.94	1.34	2.33	−0.70	0.58	0.006	−0.65	1.50	0.12

[a] At 25 °C.[21] [b] At 20 °C.[21] [c] Estimated from the intersection between absorption and emission spectra of the perylene moiety in **Py-c-PBI**; $E_{ox}(D) = +0.9$ V, $E_{red}(A) = -1.09$ V (in CH_2Cl_2 vs Fc/Fc^+); $r^+ = 3.98$, $r^- = 4.78$, $R_{cc} = 5.6$ and 17.7 Å corresponding to the stacked and extended conformations, respectively, $\lambda_i = 0.2$ eV.

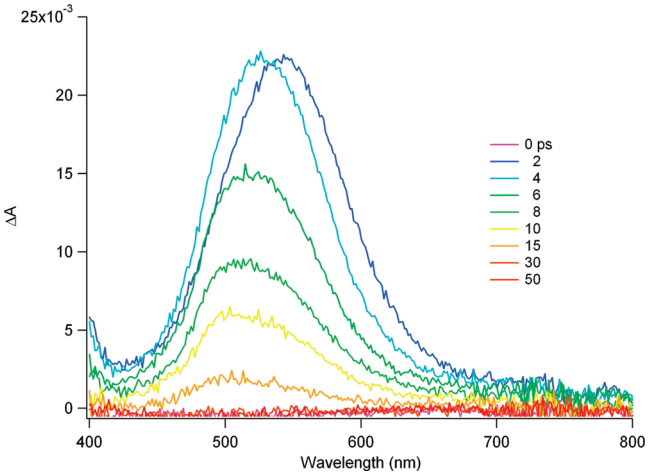

Figure 8. Femtosecond transient absorption spectroscopy of **Py-c** in THF upon 350 nm excitation. Different delay times (in ps) are indicated.

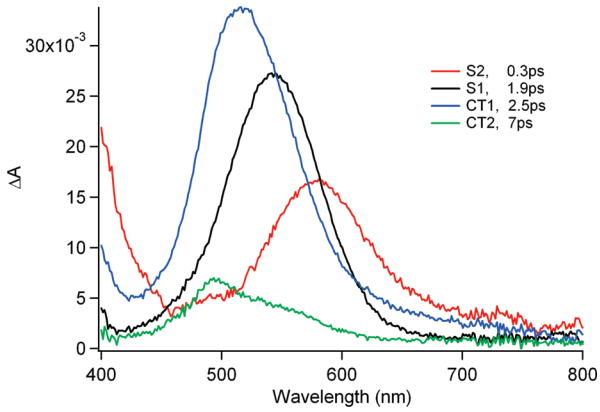

Figure 9. Evolution-associated different spectra (EADS) of **Py-c** in THF from global analysis of femtosecond transient absorption spectroscopy.

For the π-stacked conformer there is a driving force for charge separation in all solvents ($\Delta G = -0.39$ to -0.70 eV), ranging from cyclohexane to acetonitrile with a small barrier to CS ($\Delta G^{\ddagger} = 0.04-0.006$ eV). For the extended conformation the CS is endergonic in nonpolar solvents such as CHX and TOL (see Table 3). On the basis of the steady-state emission quenching and the FTA measurements, we concluded that a π-stacked conformation prevails in these two solvents since, e.g., all PBI emission is quenched. In the π-stacked conformation, pyrene acts as the donor and PBI as the acceptor.

In more polar solvents, the driving force in the extended conformation is always less than in the π-stacked one with a higher barrier, implying a slower rate of charge separation for the extended form. This slower process however is only readily observed in THF solvent and present to a minor extent in benzonitrile. Apparently, in all other solvents the $\pi-\pi$ stacking between PBI and Py is stronger than the solute−solvent interactions.

Similar to the visible excitation, also in the data obtained with UV excitation, two conformation have to be invoked. In the π-stacked conformation, ultrafast charge separation occurs, which leads to formation of a compact charge-transfer state.

In the extended form, however, a strongly competitive electron-transfer interaction between the calixarene and the pyrene occur. These processes are now faster than the interaction between Py and PBI, as the distance between these two chromophores has now strongly increased. The main process that can be observed in **Py-c-PBI** upon UV excitation at the early times in the extended conformation is the photoinduced electron transfer from the calixarene to the pyrene unit, a process that is also observed in the reference system **Py-c**. This process is very fast because of the short distance between the donor and the acceptor and is energetically allowed as well as characterized by a very small barrier to CS (see Supporting Information).

In the case of charge separation in the solvent THF, upon visible excitation, the rate constants obtained from theoretical estimates are well correlated to the global analysis results (see Table 4). It is noticed that the higher fluorescence quantum yield of **Py-c-PBI** in THF compared with those in other solvents is due to coexistence of the extended conformation, in which the photoinduced electron transfer is taking place much slower. However, it is hard to get more details of the solvent effects on the electron transfer occurring in **Py-c-PBI** as the charge separation time constants in all solvents are similar to the instrument response function (IRF; ~0.1 ps). The charge separation processes occurring in the dyad **Py-c-PBI** in THF are presented in the energy scheme (Figure 10) with excitation at 350 and 530 nm.

Formation of an extended structure is envisaged to occur by a competition of solute−solvent interactions (favoring the extended conformation) with $\pi-\pi$ interactions between pyrene and PBI (favoring the π-stacked conformation). The high polarizability of a solvent (like toluene or benzonitrile with high refractive indices) will play a role in these competitive interactions as strong polarizability plays a role in $\pi-\pi$ interactions. The exact reason why the extended form is most abundant in THF remains unclear. Most likely its H-bond accepting oxygen competes efficiently with the π-π stacking between **PBI** and **Py**, i.e. by hydrogen bonding to the amide NH on the **Py**. Also

TABLE 4: Rate Constants of Charge Separation (cs) and Charge Recombination (cr) Processes Obtained from Theoretical Estimates and Experimental Results (corresponding to 530 nm excitation) for Py-c-PBI

solvent	$\Phi_f \times 10^{-4}$	$k_{et}(s^{-1}) \times 10^{12}$ [calcd][a]	$k_{cs}(s^{-1}) \times 10^{12}$ [calcd][b]	k_{cs} (s^{-1}) $\times 10^{12}$ [exp] [c]	k_{cr} (s^{-1}) $\times 10^{10}$ [exp] [c]	k'_{cr} (s^{-1}) $\times 10^{10}$ [exp] [c]
CHX	5	0.5	2.0	10	25	5.2
TOL	12	0.2	3.2	5	10	8
THF(s)			5.7	6	1.9	
THF(e)	26	0.09	0.10	0.093	0.26	
DCM	4	0.6	6.4	10	62	6.4
ACN	5	0.5	7.0	10	71	1.1

[a] Calculated from the fluorescence quantum yield of the PBI unit. [b] Estimated using Marcus theory for π-stacked (s) and extended (e) conformers. [c] From the global and target analysis (see above).

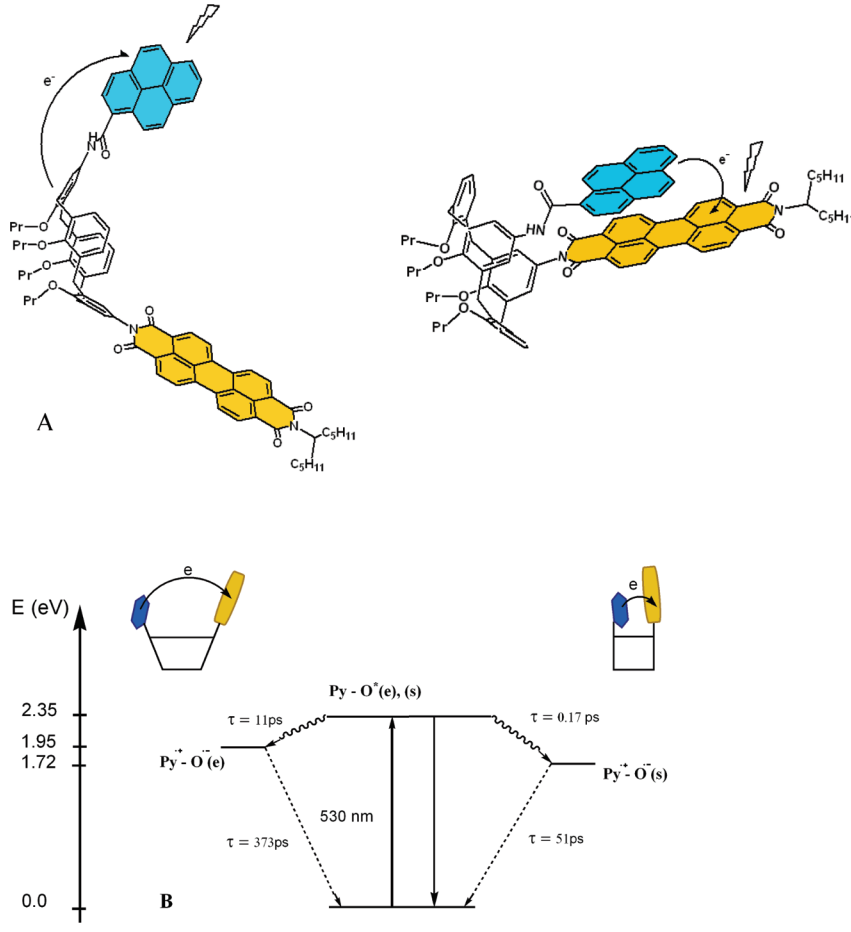

Figure 10. Schematic representation (A) of the processes occurring in the two conformations upon pyrene or perylene excitation, and energy level scheme and processes taking place in **Py-c-PBI** in THF upon PBI excitation (B). (s) and (e) are denoted for the stacked and the extended conformation, respectively.

encapsulation of THF in the calix[4]arene cavity has been observed in single crystals which may point at specific host-guest interactions that lead to a conformational change.[41] Apparently the $\pi-\pi$ interactions dominate strongly in solvents such as cyclohexane, dichloromethane, and acetonitrile, leading to the π-stacked conformation. As noted before, there is a distinct upfield shift of the pyrene ^{1}H NMR resonances (in tetrachloroethane-d_2) that is indicative for the presence of a π-stacked conformer.

Conclusions

The electron-donating pyrene and PBI acceptor have been grafted onto a calixarene scaffold. UV−vis absorption and steady-state emission indicate a strong interaction between the two chromophores, manifested by broadened absorption bands and reduced molar absorption coefficients as well as strongly quenched emission. Femtosecond transient absorption spectroscopy shows charge separation phenomena occurring on the time scale of the instrument response function (0.1 ps) and clear evidence for radical ion pair formation. The radical cation of pyrene is observed around 450 nm, and the PBI radical anion is probed in the NIR region (980 nm). Formation of the CT state occurs irrespective of solvent polarity, which has to be attributed to the preferential population of **Py-c-PBI** in a π-stacked conformation, which shows charge-transfer absorption and is characterized by optical electron transfer. This contrasts to our previously reported energy-transfer systems based on calixarene-tethered perylene bisimide dyes in which extended conformations prevailed.[8]

In THF, two excited-state decay channels are observed which indicate the presence of two conformations that are attributed to a π-stacked conformation showing fast optical charge transfer (within the 0.1 ps laser pulse excitation) and an extended conformation showing slower photoinduced electron transfer (11 ps).

Upon pyrene excitation (350 nm) in THF a fast competitive charge separation process is observed for the extended conformation, in which the pyrene now acts as the electron acceptor. In this conformation the calixarene scaffold is participating in the photoinduced interactions, taking a role as an electron donor.

Through specific solute−solvent interactions, competing with $\pi-\pi$ interactions, the extended conformation can be probed in, e.g., THF and to a minor extent in phCN. In these solvents, for both conformations a driving force for electron transfer is present.

Molecular modeling and calculations of the driving force are in accordance with the presence of a π-stacked conformation with a small center to center distance and an extended form with a larger distance and less driving force. In nonpolar solvents no driving force for electron transfer is present for the extended conformation.

The charge separation process is in good agreement with the Gibbs energy for electron transfer and the classical Marcus model. Simultaneous target analysis of the femtosecond data matrices obtained in the visible and NIR regions was performed and indicates that in THF a compact and an extended charge-transfer state are formed, which can be spectrally distinguished.

Acknowledgment. We are grateful to the NWO (de Nederlandse Organisatie voor Wetenschappelijk Onderzoek) for the grant for the femtosecond equipment and the UvA (Universiteit van Amsterdam) for structural support. We thank the Vietnamese Overseas Scholarship Program (VOSP) of the Vietnamese government for the support of NVA within the UvA-HUT project and the DFG for funding within the research training school GRK 1221 "Control of Electronic Properties of Aggregated pi-Conjugated Molecules".

Supporting Information Available: Synthesis of **Py-c-PBI**, **Py-c**, and **PBI-c**; NMR spectra of **Py-c-PBI** [(^{1}H,^{1}H)-COSY-, (^{1}H,^{13}C)-HSQC-, (^{1}H,^{13}C)-HMBC-NMR with enhanced areas]; (Photo)-physical properties of **Py-c-PBI** and **Py-c** [absorption spectra in different solvents]; absorption coefficients, fluorescence spectra, and quantum yields of **Py-c** in seven solvents; cyclic voltammograms and redox properties of **Py-c-PBI** and **Py-c**; femtosecond transient spectroscopy of **Py-c-PBI** and **Py-c** in different solvents with target analysis and SADS; 3D representation of the femtosecond data matrices of **Py-c-PBI** in THF; absorption spectra of **Py-c-PBI** in DCM together with the sum spectrum of **PBI-c** and **Py-c**; energetics for **Py-c**; lifetimes of the processes occurring in **Py-c** extracted from global and target analysis. This material is available free of charge via the Internet at http://pubs.acs.org.

References and Notes

(1) (a) Balzani, V.; Scandola, F. *Supramolecular Photochemistry*; Ellis Horwood: Chichester, U.K., 1991. (b) In *Supramolecular Dye Chemistry*; Würthner, F., Ed.; Topics in Current Chemistry 258; Springer-Verlag: Berlin, 2005.

(2) Tang, C. W. *Appl. Phys. Lett.* **1986**, *48* (2), 183–185.

(3) van Duren, J. K. J.; Yang, X.; Loos, J.; Bulle-Lieuwma, C. W. T.; Sieval, A. B.; Hummelen, J. C.; Janssen, R. A. J. *Adv. Funct. Mater.* **2004**, *14*, 403–514.

(4) Liu, Y.; Yang, Z.; Chen, Y.; Song, Y.; Shao, N *ACS Nano* **2008**, *2*, 554–560.

(5) Folmer, B. J. B.; Sijbesma, R. P.; Versteegen, R. M.; van der Rijt, J. A. J.; Meijer, E. W. *Adv. Mater.* **2000**, *12*, 874–878.

(6) Denter, U.; Buschmann, H.-J.; Knittel, D.; Schollmeyer, E. *Angew. Makromol. Chem.* **1997**, *248*, 153–163.

(7) A very recent example where cyclodextrins are combined with perylene bisimides is available:Liu, Y.; Wang, K.-R.; Guo, D.-S.; Jiang, B.-P. *Adv. Funct. Mater.* **2009**, *19*, 2230–2235.

(8) Hippius, C.; van Stokkum, I. H. M.; Gsanger, M.; Groeneveld, M. M.; Williams, R. M.; Würthner, F. *J. Phys. Chem. C* **2008**, *112*, 2476–2486.

(9) Würthner, F. *Chem. Commun.* **2004**, 1564–1579.

(10) Perylene Red is available from Exciton (www.exciton.com).

(11) In *Color Chemistry: Syntheses, Properties, and Applications of Organic Dyes and Pigments*, 3rd ed.; Zollinger, H., Ed.;VHCA and Wiley-VCH: Zürich and Weinheim, 2003.

(12) (a) Hippius, C.; van Stokkum, I. H. M.; Zangrando, E.; Williams, R. M.; Würthner, F. *J. Phys. Chem. C* **2007**, *111*, 13988–13996. (b) A simple model for **PBI-c** was recently reported: Williams, R. M. *Turk. J. Chem.* . accepted for publication.

(13) Hippius, C.; van Stokkum, I. H. M.; Zangrando, E.; Williams, R. M.; Wykes, M.; Beljonne, D.; Würthner, F. *J. Phys. Chem. C* **2008**, *112*, 14626–14638.

(14) In *Modern Molecular Photochemistry*; Turro, N. J., Ed.; University Science Books: Sausalito, CA, 1991; Chapter 5, pp 141−143. Lowry, T. H.; Richardson, K. S. Mechanism and theory in organic chemistry, 3rd ed.; Harper & Row: New York, 1987; Chapter 12, pp1000−1003.

(15) (a) In *Calixarenes*; Gutsche, D. C., Ed.; The Royal Society of Chemistry: Cambridge, U.K., 1993. (b) In *Calixarenes Revisited*; Gutsche, D. C., Ed.; The Royal Society of Chemistry: Letchworth, 1998.

(16) (a) Kim, S. K.; Bok, J. H.; Bartsch, R. A.; Lee, J. Y.; Kim, J. S. *Org. Lett.* **2005**, *7*, 4839–4842. (b) Lee, S. H.; Kim, S. H.; Kim, S. K.; Jung, J. H.; Kim, J. S. *J. Org. Chem.* **2005**, *70*, 9288–9295. (c) Schazmann, B.; Alhashimy, N.; Diamond, D. *J. Am. Chem. Soc.* **2006**, *128*, 8607–8614. (d) Kim, H. J.; Quang, D. T.; Hong, J.; Kang, G.; Hamb, S.; Kim, J. S. *Tetrahedron* **2007**, *63*, 10788–10792.

(17) Nishimura, Y.; Takemura, T.; Arai, S. *ARKIVOC* **2007**, (xiii), 259–268.

(18) Demas, J. N.; Crosby, G. A. *J. Phys. Chem.* **1971**, *75*, 991–1024.

(19) Ford, W. E.; Kamat, P. V. *J. Phys. Chem.* **1987**, *91*, 6373–6380.

(20) Eaton, D. F. *Pure Appl. Chem.* **1988**, *60*, 1107–1114.

(21) (a) van Stokkum, I. H. M.; Larsen, D. S.; van Grondelle, R. *Biochim. Biophys. Acta* **2004**, *1657*, 82–104. (b) van Stokkum, I. H. M.; Lozier, R. H. *J. Phys. Chem. B* **2002**, *106*, 3477–3485. (c) Mullen, K. M.; van Stokkum, I. H. M. *J. Stat. Software* **2007**, *18* (3); URL: http://www.jstatsoft.org/v18/i03/. (d) Global and target analysis can be performed with, e.g., the R package TIMP; see http://cran.r-project.org/doc/packages/TIMP.pdf.

(22) Prins, J.; Jollif, K. A.; Hulst, R.; Timmerman, P.; Reinhoudt, D. N. *J. Am. Chem. Soc.* **2000**, *122*, 3617–3627.

(23) In *Handbook of Photochemistry*, 3rd ed.; Montalti, M., Credi, A., Prodi, L., Gandolfi, M. T., Eds.; CRC/Taylor & Francis: New York, 2006;

(24) Yao, C.; Kraatz, H.; Steer, R. P. *Photochem. Photobiol. Sci.* **2005**, *4*, 191–199.

(25) (a) Ford, W. E.; Hiratsuka, H.; Kamat, P. V. *J. Phys. Chem.* **1989**, *93*, 6692–6696. (b) Salbeck, J.; Kunkely, H.; Langhals, H.; Saalfrank, R. W.; Daub, J. *Chimia* **1989**, *43*, 6–9.

(26) Veldman, D.; Chopin, S. M. A.; Meskers, S. C. J.; Groeneveld, M. M.; Williams, R. M.; Janssen, R. A. J. *J. Phys. Chem. A* **2008**, *112*, 5846–5857.

(27) (a) Sautter, A.; Kaletaş, B. K.; Schmid, D. G.; Dobrawa, R.; Zimine, M.; Jung, G.; van Stokkum, I. H. M.; De Cola, L.; Williams, R. M.; Würthner., F. *J. Am. Chem. Soc.* **2005**, *127*, 6719–6729. (b) Kaletas, B. K.; Dobrawa, R.; Sautter, A.; Würthner, F.; Zimine, M.; De Cola, L.; Williams, R. M. *J. Phys. Chem. A* **2004**, *108*, 1900–1909. (c) Kawai, K.; Takada, T.; Tojo, S.; Ichinose, N.; Majima, T. *J. Am. Chem. Soc.* **2001**, *123*, 12688–12689. (d) Daub, J.; Engl, R.; Kurzawa, J.; Miller, S. E.; Schneider, S.; Stockmann, A.; Wasielewski, M. R. *J. Phys. Chem. A* **2001**, *105*, 5655–5665. (e) Liu, A.; Sauer, M. C., Jr.; Loffredo, D. M.; Trifunac, A. D. *J. Photochem. Photobiol., A* **1992**, *67*, 197–208. (f) Kira, A.; Imamura, M.; Shida, T. *J. Phys. Chem.* **1976**, *80*, 1445–1448. (g) Schomburg, H.; Staerk, H.; Weller, A. *Chem. Phys. Lett.* **1973**, *22*, 1–4. (h) Richards, J. T.; West, G.; Thomas, J. K. *J. Phys. Chem.* **1970**, *74*, 4137–4141.

(28) (a) Foggi, P.; Pettini, L.; Righini, R.; Califano, S. *J. Phys. Chem.* **1995**, *99*, 7439–7445. (b) Raytchev, M.; Pandurski, E.; Buchvarov, I.; Modrakowski, C.; Fiebig, T. *J. Phys. Chem. A* **2003**, *107*, 4592–4600. See also refs 27a, 27b, and 27d.

(29) (a) Okada, T.; Karaki, I.; Mataga, N. *J. Am. Chem. Soc.* **1982**, *104*, 7191. (b) Shida, T. *Electronic Absorption Spectra of Radical Ions*; Elsevier: New York, 1988. (c) Richards, J. T.; West, G.; Thomas, J. K. *J. Phys. Chem.* **1970**, *74*, 4137.

(30) Neuwhal, F. V. R.; Foggi, P. *Laser Chem.* **1999**, *19*, 375–379. See also ref 27a.

(31) Fiebig, T.; Stock, K.; Lochbrunner, S.; Riedle, E. *Chem. Phys. Lett.* **2001**, *345*, 81–88.

(32) (a) Shibano, Y.; Umeyama, T.; Matano, Y.; Tkachenko, N. V.; Lemmetyinen, H.; Araki, Y.; Ito, O.; Imahori, H. *J. Phys. Chem. C* **2007**, *111*, 6133–6142. (b) Wolffs, M.; Delsuc, N.; Veldman, D.; Van Anh, N.; Williams, R. M.; Meskers, S. C. J.; Janssen, R. A. J.; Huc, I.; Schenning, A. P. H. J. *J. Am. Chem. Soc.* **2009**, *131* (13), 4819–4829. (c) Veldman, D.; Chopin, S. M. A.; Meskers, S. C. J.; Groeneveld, M. M.; Williams, R. M.; Janssen, R. A. J. *J. Phys. Chem. A* **2008**, *112*, 5846.

(33) Schuddeboom, W.; Scherer, T.; Warman, J. M.; Verhoeven, J. W. *J. Phys. Chem.* **1993**, *97*, 13092–13098.

(34) Weller, A. *Z. Phys. Chem., Neue Folge (Wiesbaden)* **1982**, *133*, 93–98.

(35) Oevering, H.; Paddon-Row, M. N.; Heppener, M.; Oliver, A. M.; Cotsaris, E.; Verhoeven, J. W.; Hush, N. S. *J. Am. Chem. Soc.* **1987**, *109*, 3258–3269.

(36) In *Lange's Handbook of Chemistry, 70th Anniversary*, 16th ed.; Speight, J. G., Ed.; Mcgraw-Hill Education: United States, 2005.

(37) Langhals, H. *Chem. Phys. Lett.* **1988**, *150*, 321–324.

(38) Similar *A* factors are reported in the following:(a) Williams, R. M.; Koeberg, M.; Lawson, J. M.; An, Y.-Z.; Rubin, Y.; Paddon-Row, M. N.; Verhoeven, J. W. *J. Org. Chem.* **1996**, *61*, 5055–5062. (b) In *Principles of Molecular Photochemistry, An Introduction*; Turro, N. J., Ramamurthy, V., Scaiano, J. C., Eds.; University Science Books: Sausalito, CA, 2009; p 428.

(39) Marcus, R. A.; Sutin, N. *Biochim. Biophys. Acta* **1985**, *811*, 265.

(40) Similar internal reorganization has been used:Beckers, E. H. A.; Meskers, S. C. J.; Schenning, A. P. H. J.; Chen, Z.; Würthner, F.; Janssen, R. A. J. *J. Phys. Chem. A* **2004**, *108*, 6933–6937.

(41) Shahgaldian, P.; Coleman, A. W.; Rather, B.; Zaworotko, M. *J. Inclusion Phenom. Macrocyclic Chem.* **2005**, *52*, 241.

JP9055279